Low-cost 3D Wind Anemometers for Architectural Wind Modeling and Prediction

J. Hirano* and D. Garmire**

*University of Hawaii at Manoa, Honolulu, HI, USA, jhirano@hawaii.edu
**University of Hawaii at Manoa, Honolulu, HI, USA, garmire@hawaii.edu

ABSTRACT

With the advancement in distributed power generation and growth of the sustainability movement there has been time and money spent on small-scale wind turbine generation. This movement has created a need for the detailed studying and surveying of small-scale wind patterns and architectural wind. The greatest challenge of this field is gathering high-resolution data in both the spatial and time domains with an array of sensors that are affordable and deployable by the individual or business. In response to this need, we developed a low-cost three-dimensional wind anemometer. Our device is designed to be a low-cost solution for taking high spatial resolution of areas near and on building structures. This article describes and analyzes our initial concepts and designs. We were able to produce prototypes capable of measuring wind speeds over 100 mph in 3D at 1kHz sampling and a precision down to 0.2 mph. We also discuss an approach to mass-producing the device and deployment techniques.

Keywords: anemometer, architectural wind, microsensors

1 INTRODUCTION

In recent years there has been a growth in the field of distributed energy generation [1]. This growth is being spurred not only in suburban but also urban areas. One of the main sources of energy is from small-scale wind turbines. These turbines are designed to harvest energy from both the wind at high altitudes, on top of large buildings, and the architectural wind. Architectural wind is the natural channeling of wind due to the topology of buildings [2, 3]. This topology can cause a magnified velocity of wind in a particular direction, generally along the vertical axis. A question then arises as to how to optimize the design and distribution of architectural wind turbines [4, 5], for not only cities but also residential areas. In our search for a way to study architectural wind we found a lack of affordable sensors to monitor this wind behavior. To study this type of wind behavior we required an array of three-dimensional (3D) anemometers that has high resolution in time and space. High-frequency sampling is needed because turbulence in the air fluctuates on the order of 100 Hz as shown in adaptive optics for astronomy and free-space communication [6]. A conventional 3D anemometer costs in the range of about $2,500 making a distributed system expensive. Therefore, a sensor was necessary to determine wind velocity as a 3D vector while still being low-cost and easy to deploy around a building.

1.1 Device Theory

The 3D anemometer is designed based on the principles of mass-spring physics. In the case of our design, the wind provides a force against the device which has an inherent spring constant, *K*, and the wind-catching component has some mass, *M*, and coefficient of drag, *D*, which is linearly dependent on wind velocity for low Reynolds number (ratio of inertial forces to viscous forces). The sensor element should have high drag to maximize the transduction of wind energy to elastic energy and reduce vibration but has low cross-sectional area to minimize altering the large-scale wind patterns. The proof mass should also be chosen as spherical in shape and semi-porous to reduce turbulent effects. A small proof mass also helps reduce turbulence due to a decreased Reynolds number. The three-stage parallel-guided suspension is designed to have approximately the same stiffness in all three directions and high rotational stiffness. For a parallel-guided suspension, the stiffness, *K*, can be described by the formula:

$$\text{Stiffness: } K = 2w(t/L)^3 E, \quad (1)$$

where *t*, *w*, and *L* are the thickness, width, and length of each beam in the suspension and *E* is the Young's Modulus of the material (roughly 2.3GPa for plastic). The force is determined by the displacement of the center column from its initial state. The displacement is measured as a voltage signal controlled by an infrared emitter-collector pair. The displacement along each axis is taken independently to determine the forces in each direction. The voltages are translated back into a quantitative value representing the speed of the wind in each of the three orthogonal directions. The sensor proximity and sensitivity and suspension length and therefore deflection and resonant frequency can be optimized together to obtain the best signal-to-noise ratio and accuracy for the given manufacturing constraints.

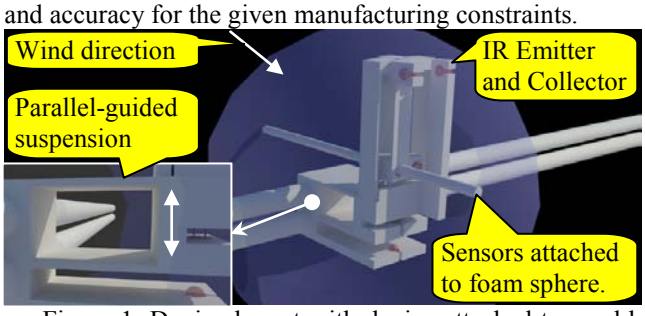

Figure 1: Device layout with device attached to a cable with three parallel-guided suspensions in series.

2 PROOF OF CONCEPT

The initial prototype was a macro scale design using readily available materials. Figure 2 gives an image of the initial prototype. Its design can be broken up into three regions. Region 1 is the mass that the wind acts upon to transfer its energy to the rest of the sensor. Region 2 is the center shaft designed to measure the force in the x and y directions. Region 3 is the base structure which was designed to stabilize the sensor and measure the force in the z direction. Along each axis infrared LED pairs are used to determine the displacement in the particular axis. Figure 2 also shows a schematic of the configuration of the LED, phototransistor, operational amplifier, and resistors used in each of the axes. The reason for the op-amp is to amplify the changes in the voltage of the phototransistor.

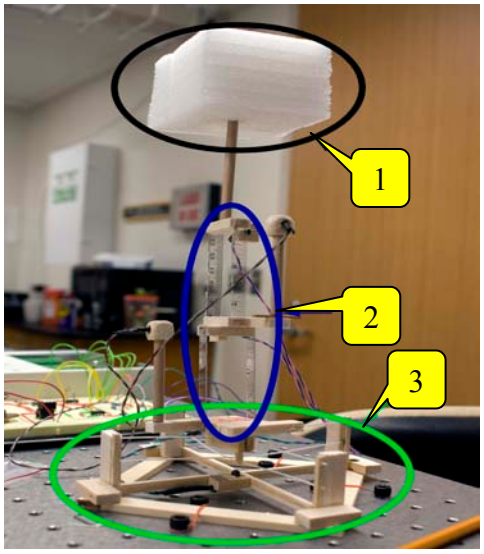

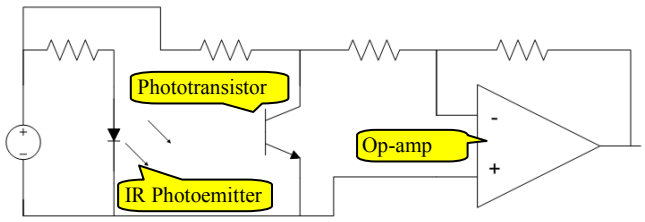

Figure 2. Initial prototype (top) and circuit schematic (bottom) to determine the displacement

2.1 Experiment

Tests on the sensor were done in a controlled lab environment. Voltage data was collected with 1 kHz sampling using a National Instrument DAQ interfaced with Matlab. The wind source was a compressed air can that outputs at about 50mph. The wind source was calibrated first on a hand-held anemometer. The first test on the sensor was a controlled wind source approaching in a positive x direction. The wind source was placed 1 cm away from the proof mass of the device, in order to deliver the greatest amount of force. The air was dispersed in a 2 second increment. The second test examined the physical limits of the device. In this test, an increasing force was applied to each of the three axes individually.

2.2 Results

The results of the first test are shown in Figure 3. For wind approaching 50mph, we had a voltage output of 45mV. From this data set we found that with no wind we have three standard deviations of 0.18mV which gives the sensor a precision of about 0.2mph. From this graph we also see that the response time to the wind is almost immediate whereas in conventional propeller-style anemometers it takes some time to accelerate and reach the same output. Note that there is coupling between axes; however, this coupling can be compensated for in the programming of wind velocity and in the device redesign.

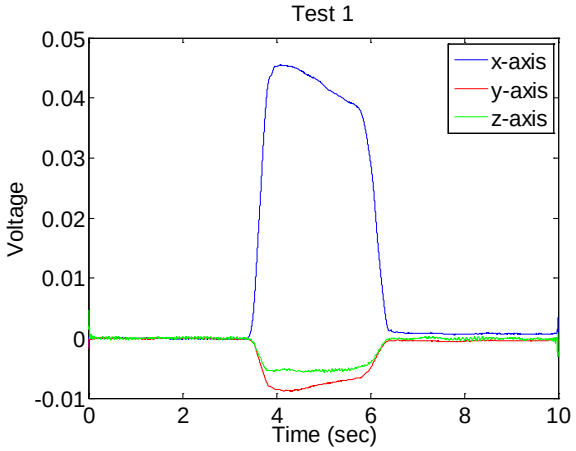

Figure 3. Test 1 – Single directional Wind

The second sequence of tests produced the data in Figure 4. From the data we see that in the y and x directions the max value is around 100mV, about twice the magnitude of the first test. This measurement implied that the max wind speed was about 100mph.

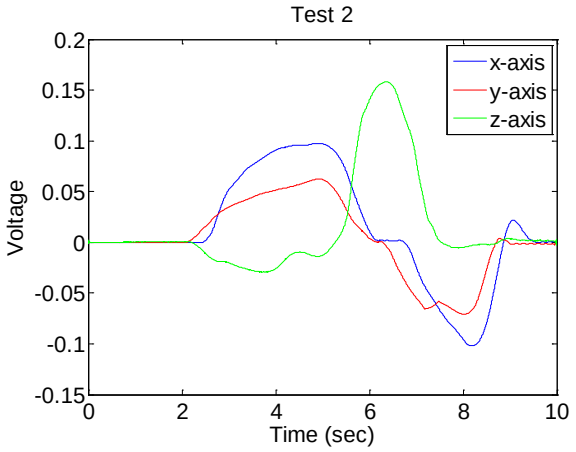

Figure 4. Test 2 – Physical Constraints Test

Clean Technology 2010, www.ct-si.org, ISBN 978-1-4398-3419-0

3 NEW DEVICE

The second prototype is a scaled down version of the original design. Some modifications to the design addressed some of the issues with the original prototype. This version was fabricated using a fused deposition modeling (FDM) process in Acrylonitrile Butadiene Styrene (ABS). This second prototype was placed through a series of tests to calibrate the device.

3.1 Calibration

We calibrated the 3D anemometer through a series of lab tests. The first test mapped the voltage output based on a known displacement in the positive direction. This test was set up using an adjustable optical platform, used to move the top of the sensor a fixed distance from its center. On the platform a probe arm extended to the device in order to move the sensor. The arm was set to make contact with the center of the mass attached to the top of the center structure. The placement represents an average of the displacement of the top and the bottom of the mass. Each of the measurements had 1 millimeter incremental changes in the positive x-direction.

The second part of the calibration sequence used a controlled wind force to apply a real world simulation on the device. Using an air compressor and a series of tubes and valves, an artificial wind source was created and channeled to two separate outputs. To calibrate the wind source, two handheld anemometers were initially placed at each outlet of the wind source. After a series of adjustment both streams of air were producing the same velocity of wind with matching values at each of the outputs. At this point one of the anemometers was replaced with our sensor for direct comparison. The wind force was applied by ramping the release of air from an initial zero state. Sequences of different wind speeds were applied to the device.

In the final calibration test, the limits of the structure were tested showing the maximum wind velocities that the prototype could measure in each direction without failing.

3.2 Results

In the first test sequence (Figure 5), we saw a steady increase in output voltage with the increase in displacement in the positive direction. For this test the displacement started at 0mm and increased to 7mm. From Figure 5, it is shown that there were some linear steps from one displacement to the next. There were some discrepancies between 3 through 5 where the steps seem to be larger then the other steps. This linearity held from 0 to almost 10mV or a 7mm displacement.

We ran the simulated wind test with steadily increasing wind speeds. In Figure 6, we see three particular cases with maximum wind speeds of 5.0, 10.2, 13.5, 18.4, and 23.8mph. The reason for the ramping of the wind velocity was to allow the system to sense a larger wind velocity on the sensor. The data shows that with the increase of velocity there was a steady increase in the voltage output of the system. As shown by Figure 6, for a wind velocity of about 23.8mph the sensor produced an output voltage of about 6mV. These results show that we can reach speeds approaching 100mph, which is about 25mph wind speeds at 6mV since we have linearity as we approach 20mV. The 23.8mph plot may represent an even higher velocity because the hand-help anemometers used a propeller approach which has a measurement lag so a quick burst of wind will not fully be read.

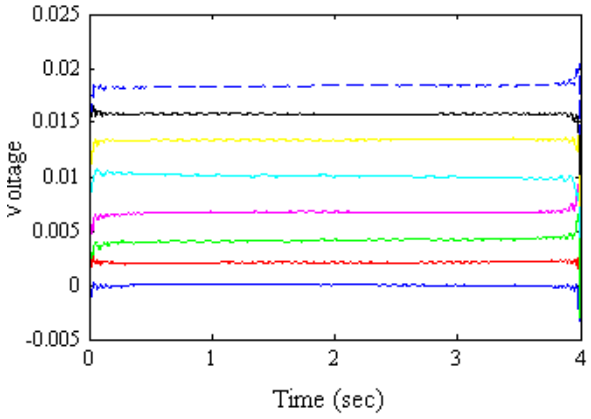

Figure 5. Displacement along the positive x-axis

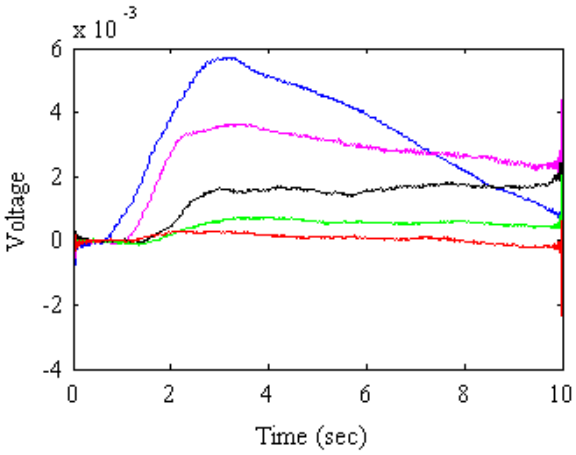

Figure 6. Ramping incoming wind along Positive X-Axis

In the final test (Table 1), we see that the maximum voltage in the x-axis was about 50mV, while the maximum voltage for the y-axis was only 28.9mV (due to some prior damage). Assuming the linearity between voltage and wind speed held, the maximum sustained wind speed was over 100mph in both the x and the y directions.

	Max (mV)	Min (mV)
X Direction	50.6	-47.4
Y Direction	28.9	-41.0

Table 1. Physical Limits in X and Y Axes

3.3 Discussion

For the data collected through the series of experiments we see that the new device holds many of the same properties of the original prototype. As seen in the first two tests, we have linearity between the displacement of the force applied to the proof mass and the output voltage. The second prototype was also able to meet the maximum wind speed of the proof-of-concept design.

The tests have shown that there is room for optimization in different areas. One of the key improvements is in the design of the suspension system. As shown from Figure 5, the increase in voltage output to displacement is non-linear but can be easily modeled. This available displacement and voltage output compared to the maximum wind speed means that the supporting beams could be relaxed in the moving direction while stiffened in the counter direction. This approach will allow for a greater signal-to-noise ratio than previously attained.

From Figure 7 it can be seen that there is turbulence present. This turbulence is due to the direct use of the air compressor. To improve the test results and the calibration process we can implement two identical miniature wind tunnels. One set aside for the calibrating anemometer and the other for the sensor, this approach will eliminate the noise in the signal due to the turbulence. Also to optimize the test we can use a larger air compressor or an alternative wind source. The size of the air compressor limits the constant stream of higher wind velocities applied to the device.

4 CONCLUSION

From the preliminary prototype we showed that a device based on a mass-spring system is able to detect and determine the wind velocity and direction in a three-dimensional vector. The proof of concept testing also showed that our design behaved linearly with the increase in wind velocity. This device also was able to handle wind speed up to 100mph with a precision of 0.2mph. The second prototype was able to maintain the characteristics of the original in a smaller package.

4.1 Future Enhancements

We are looking to move into the next phase of design, which will properly address the low cost aspect of the project. This phase includes incorporating the optimizations suggested earlier in the paper and applying them to the low-cost process of injection molding. This approach will allow us to create the device at a lower cost and at a higher production rate. Figure 8 shows the initial design of how we would go about creating such a sensor. The new design breaks down the sensor into three individual parts that can be quickly assembled. There are more considerations such as finding another IR transistor pair, preferably smaller, that will allow for modification in the design. Changing the infrared phototransistors would allow the possibility of creating custom integrated circuits to minimize the size of the sensor, thereby increasing its portability.

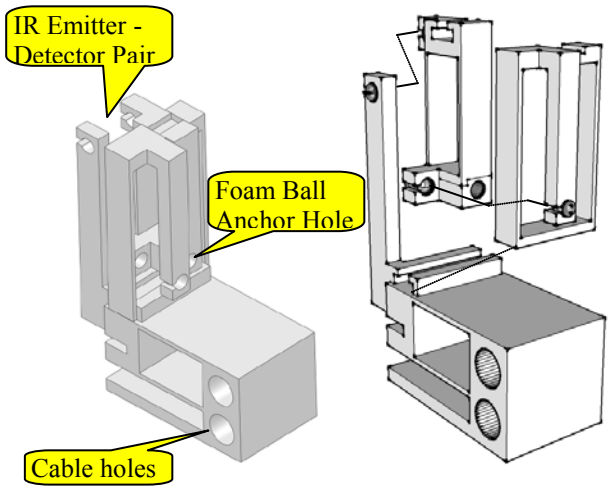

Figure 8. Prototype 3 Injection Molding Assembly (left) with a breakdown into 3 injection moldable parts (right)

With the production of a multitude of sensors we can expand and implement a distributed sensor network. The network of sensors allows for the examination of the patterns in the wind and how it changes as it approaches and travels around building topology. With this distributed network come the challenges of looking at different methods of large-scale networking and the possible comparisons of wired/bus networks with wireless networks.

REFERENCES

[1] T. Ackermann, G. Andersson, and L. S\öder, "Distributed generation: a definition," *Electric Power Systems Research* 57, no. 3 (2001): 195–204.

[2] J. J Kim and J. J Baik, "A numerical study of the effects of ambient wind direction on flow and dispersion in urban street canyons using the RNG k–ε turbulence model," *Atmospheric Environment* 38, no. 19 (2004): 3039–3048

[3] David Hamlyn and Rex Britter, "A numerical study of the flow field and exchange processes within a canopy of urban-type roughness," *Atmospheric Environment* 39, no. 18 (June 2005): 3243-3254.

[4] S. Li et al., "Using neural networks to estimate wind turbine power generation," *IEEE Transactions on Energy Conversion* 16, no. 3 (2001): 276–282.

[5] Q. Chen, "Using computational tools to factor wind into architectural environment design," *Energy & Buildings* 36, no. 12 (2004): 1197–1209.

[6] J.W. Hardy, Adaptive Optics for Astronomical Telescopes, 1998. (page 26)